Journal of Hydrology 528 (2015) 631–642

Contents lists available at ScienceDirect

Journal of Hydrology

journal homepage: www.elsevier.com/locate/jhydrol

Effect of baseline meteorological data selection on hydrological modelling of climate change scenarios

Renji Remesan, Ian P. Holman *

Cranfield Water Science Institute, Cranfield University, United Kingdom

ARTICLE INFO

Article history:
Received 5 December 2014
Received in revised form 27 May 2015
Accepted 14 June 2015
Available online 9 July 2015
This manuscript was handled by Konstantine P. Georgakakos, Editor-in-Chief, with the assistance of Matthew McCabe, Associate Editor

Keywords:
Uncertainty
TRMM3B42 V7
Aphrodite
Impact response surface
Evapotranspiration
Climate change

SUMMARY

This study evaluates how differences in hydrological model parameterisation resulting from the choice of gridded global precipitation data sets and reference evapotranspiration (ETo) equations affects simulated climate change impacts, using the north western Himalayan Beas river catchment as a case study. Six combinations of baseline precipitation data (the Tropical Rainfall Measuring Mission (TRMM) and the Asian Precipitation – Highly Resolved Observational Data Integration Towards Evaluation of Water Resources (APHRODITE)) and Reference Evapotranspiration equations of differing complexity and data requirements (Penman–Monteith, Hargreaves–Samani and Priestley–Taylor) were used in the calibration of the HySim model. Although the six validated hydrological models had similar historical model performance (Nash–Sutcliffe model efficiency coefficient (NSE) from 0.64 to 0.70), impact response surfaces derived using a scenario neutral approach demonstrated significant deviations in the models' responses to changes in future annual precipitation and temperature. For example, the change in Q10 varies between −6.5% and −11.5% in the driest and coolest climate change simulation and +79% to +118% in the wettest and hottest climate change simulation among the six models. The results demonstrate that the baseline meteorological data choices made in model construction significantly condition the magnitude of simulated hydrological impacts of climate change, with important implications for impact study design.

© 2015 The Authors. Published by Elsevier B.V. This is an open access article under the CC BY-NC-ND license (http://creativecommons.org/licenses/by-nc-nd/4.0/).

1. Introduction

Understanding the current and future temporal dynamics of the hydrological behaviour of rivers is vital for management of hydro-power generation, irrigation systems, public water supply and flood control structures (Jain et al., 2010). However, there is a widely recognised cascade of uncertainty in top-down climate change impact studies (Wilby and Dessai, 2010) that affects the certainty in future water resource assessments (Refsgaard et al., 2007). Many elements of the uncertainty cascade within climate impacts modelling have been quantitatively assessed, highlighting the uncertainty associated with climate model (RCMs or GCMs) choice (Fowler and Kilsby, 2007; Woldemeskel et al., 2012), emissions scenario (Maurer, 2007), downscaling method, model choice, etc. (Pappenberger and Beven, 2006; Buytaert et al., 2009; Kay et al., 2009; Chen et al., 2011; Xu, 1999; Wilby et al., 2004; Wood et al., 2004).

However, quantification of the hydrological impacts of climate change requires quality baseline data to enable meaningful comparison between present and future, but there is a paucity or lack of coverage of land based measurements of meteorological variables in many parts of the world. Data sparsity tends to be exacerbated in mountainous regions where very steep temperature and precipitation gradients are poorly characterised by the limited spatial and temporal extents of raingauge and weather station networks (Legates and Willmott, 1990), leading to significant uncertainty in precipitation and evapotranspiration.

Recently, many global/regional datasets have been developed as an alternative or supplement to ground-based data over basins with severe climate data scarcity (Meng et al., 2014) for use in hydrological modelling studies (Andermann et al., 2012; Meng et al., 2014). These data sets include the Asian Precipitation – Highly Resolved Observational Data Integration Towards Evaluation of Water Resources (APHRODITE) data and satellite-based precipitation products such as the Tropical Rainfall Measuring Mission (TRMM). However, there are considerable temporal and spatial differences between such data products in comparison to weather station precipitation (Tian et al., 2007; Habib et al., 2009; Andermann et al., 2011; Li et al., 2012; Lu

* Corresponding author at: Cranfield Water Science Institute, Cranfield University, Cranfield, Bedford MK43 0AL, United Kingdom.
E-mail address: i.holman@cranfield.ac.uk (I.P. Holman).

http://dx.doi.org/10.1016/j.jhydrol.2015.06.026
0022-1694/© 2015 The Authors. Published by Elsevier B.V.
This is an open access article under the CC BY-NC-ND license (http://creativecommons.org/licenses/by-nc-nd/4.0/).

et al., 2013; Jamandre and Narisma, 2013), although these may partly be due to the difficulties in gauge-radar assimilation or comparison (Vasiloff et al., 2009). A number of studies have used TRMM and APHRODITE for hydrological simulation in large river catchments whilst also detailing their uncertainties – for example, Collischonn et al. (2007, 2008) used TRMM rainfall data in modelling the Tapajós river basin in Brazil; and APHRODITE precipitation data were used in hydrological modelling of the Aksu River basin, North-Western China (Zhao et al., 2013) and Himalayan rivers in Nepal (Andermann et al., 2012). Meng et al. (2014) highlighted that TRMM (3B42V6) daily data sets were more appropriate for monthly hydrological modelling in hilly regions of the Tibetan Plateau within the Yellow river basin, but studies by Xue et al. (2013) have shown a clear improvement of 3B42V7 data sets over 3B42V6 in hydrological applications in the Wangchu Basin in Bhutan. Their study demonstrated that 3B42V7 provided better basin-scale agreement with observed (2001–2010) monthly and daily rain gauge data and improved rainfall intensity distribution than 3B42V6. Andermann et al. (2011) compared APHRODITE with TRMM-3B42 (and 3B43 data) along with other remote sensing based precipitation datasets along the Himalayan front and suggest that estimation of precipitation in high elevations regions such as the Himalaya is challenging and that significant inconsistencies exist between different remote sensing data products.

The quantification of Reference Evapotranspiration (ETo) is also associated with significant uncertainties that can affect water and energy budgeting. Recent PET based studies including FLUXNET (Baldocchi et al., 2001) and LandFlux-EVAL (Mueller et al., 2011, 2013) have addressed evapotranspiration uncertainty quantification and evaluation. These studies principally aimed to compare satellite-based estimates, IPCC AR4 simulations, land surface model (LSM) simulations and reanalysis data products to produce an ensemble of global benchmark PET datasets. Kay and Davies (2008) found important differences between ETo estimates using Penman–Monteith, a simpler temperature-based potential evapotranspiration (PET) method and the UK Meteorological Office Rainfall and Evapotranspiration Calculation System (MORECS) when applied to data from five global and eight regional climate models. However, whilst Thompson et al. (2014) have demonstrated that the choice of ETo method affected the simulated hydrology of the Mekong and Andermann et al. (2011) highlighted the significant inconsistencies that exist between different precipitation data products, including APHRODITE with TRMM-3B42 (and 3B43 data), no studies have assessed the combined effects of these two uncertainties for future climate change simulations. There is therefore a lack of understanding concerning the effect that the modeller's subjective choice of historical meteorological data, as determined by their selection of both baseline weather data products and the methods to derive meteorological variables such as ETo, have on the uncertainty in future hydrological impacts.

This study evaluates how the choice of gridded global precipitation data sets and reference evapotranspiration (ETo) method affects baseline hydrological model parameterisation and thereby the uncertainty in simulated future climate change impacts using scenario-neutral impact response surfaces. Six combinations of baseline daily precipitation datasets (TRMM and APHRODITE) and ETo methods (Penman–Monteith, Hargreaves–Samani and Priestley–Taylor) were used in the calibration/validation of the HySim model (Manley and Water Resource Associates Ltd., 2006), using the north western Himalayan Beas river catchment as a case study.

2. Study area and methods

The Beas River is one of the five major rivers of the Indus basin in India and originates in the Himalayas, flowing for approximately 470 km before joining the Sutlej River. The catchment area, upstream of the Pong reservoir, is around 12,560 km^2, and varies in elevation from 245 to 6617 metres above sea level (m asl). The catchment is bounded by Latitude 31°28′–32°26′N and Longitude 75°56′–77°48′E (Fig. 1). Soils in the catchment are young and relatively thin, with their thickness increasing in the valleys and areas with gentle slopes (Pandey, 2002). The major land cover classes include forest, snow and bare rock, with about 65% of the area covered with snow during winter (Singh and Bengtsson, 2003). The Beas catchment is under the influence of western disturbances that bring snowfall to the upper sub-catchment during winter (December–April), whilst the monsoon provides around

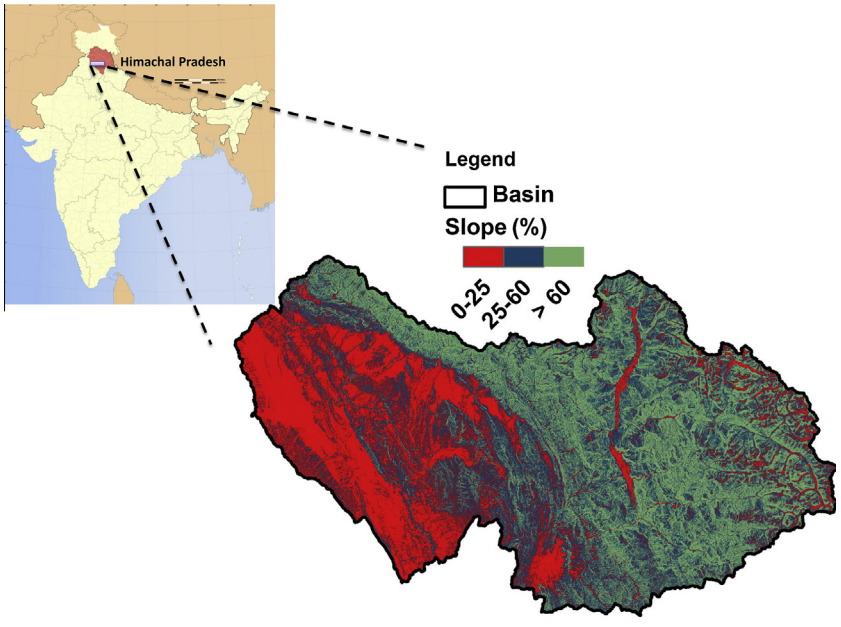


Fig. 1. The study area of the Beas river basin in northern India.

70% of the annual rainfall during June–September. The catchment is characterised by moderate – low temperatures with mean minimum and mean maximum winter temperatures of −1.6 °C and 7.7 °C, respectively (Singh and Ganju, 2008). The Pong reservoir provides an active storage capacity of 7051 Mm^3 to support flood protection, hydropower generation and almost 9000 Mm^3/year of irrigation water demands (Jain et al., 2007). Daily gauged reservoir inflows from January 1998 to December 2008 (11 years) were used in this study.

The methodology adopted in this study for analysis of uncertainty propagation is shown in Fig. 2. Six HySim models employing different combinations of two gridded precipitation data sets and three evapotranspiration equations (Sections 2.1 and 2.2) have been calibrated and validated against observed daily river discharge data (Section 2.4). Then a scenario-neutral approach has been adopted to study the propagation of uncertainties in the HySim models. The methodology departs from conventional GCM/RCM based scenario-led impact studies because it is based on sensitivity analyses of catchment responses to a plausible range of climate changes, avoiding the application of time varying GCM/RCM scenario outcomes simulated under certain assumptions of social/economic/environmental policies, thus making it scenario-neutral (Prudhomme et al., 2010). Within the Scenario-neutral approach, a range of annual temperature changes and annual precipitation changes (Section 2.5) are applied to the baseline (2000–2008) weather. Each of the six HySim model were then run with each of the modified weather time series, and their changes in hydrological indicators plotted as impact response surfaces [a surface plot showing the variation of a certain quantity (e.g.: surface runoff) across the ranges of plausible changes in future temperature and precipitation].

2.1. Rainfall and meteorological data

This study has used three datasets – two gridded precipitation datasets and a gridded meteorological dataset:

- *Tropical Rainfall Measuring Mission (TRMM)* Data product 3B42 V7 of daily precipitation data has been used in this study. TRMM is a joint space programme between NASA and the Japanese space agency to monitor precipitation in the tropics and subtropics and its associated latent heat (launched on November 27, 1997) which provides an important precipitation database for environmental and hydrological research around the globe. The gridded TRMM data at a spatial resolution of 0.25° × 0.25° over the latitudinal band of 50° N–S are available from 1998.
- *Asian Precipitation – Highly Resolved Observational Data Integration Towards Evaluation of Water Resources (APHRODITE)*– the APHRODITE Water Resources project (http://www.chikyu.ac.jp/precip/) has created long-term daily gridded precipitation datasets over Asia from the year 1951. In this study we have used 0.25° × 0.25° gridded daily datasets over Monsoon Asia (APHRO_MA_V1101), available between 60°E–150°E and 15°S–55°N, which are calculated by interpolation of rain-gauge data from meteorological stations in the region (Yatagai et al., 2012).
- *NCEP Climate Forecast System Reanalysis (CFSR)* data – meteorological variables (e.g.: daily maximum temperature, daily minimum temperature, daily wind velocity, daily average relative humidity, daily average solar radiation, etc.) at a spatial resolution of 0.5° × 0.5° are available from the National Centres for Environmental Protection (NCEP) Climate Forecast System Reanalysis (CFSR) for the 31-yr period from 1979 to 2009 for the calculation of ETo.

2.2. Potential evapotranspiration equations

There are numerous methods available for the calculation of evapotranspiration, which differ in their data requirements and accuracy (see the reviews by Kumar et al. (2011) and Kumar et al. (2012)). In this study we have used three reference evapotranspiration equations of differing complexity in input data usage and process representation for the calculation of ETo viz. FAO Penman–Monteith (Allen et al., 1998), Hargreaves–Samani (Hargreaves and Samani, 1985a,b) and Priestley–Taylor (Priestley and Taylor, 1972).

2.2.1. The FAO Penman–Monteith method

The FAO Penman–Monteith method is considered as one of the best methods for ETo calculation (Ngongondo et al., in press), but also has the greatest data demands. It considers both aerodynamic phenomena and surface resistance factors (resistance of vapour flow through the transpiring vegetation and evaporating soil surface) (Allen et al., 1998). The equation is given as

$$ET_0 = \frac{0.408\Delta(R_n - G) + \gamma \frac{900}{T+273} u_2 (e_s - e_{a)}}{\Delta + \gamma(1 + 0.34u_2)} \quad (1)$$

where ET_0 is reference evapotranspiration (mm day^{-1}), R_n net radiation at the crop surface (MJ m^{-2} day^{-1}), G soil heat flux density (MJ m^{-2} day^{-1}), T mean daily air temperature at 2 m height (°C), u_2 wind speed at 2 m height (m s^{-1}), e_s saturation vapour pressure (kPa), e_a actual vapour pressure (kPa), $(e_s - e_a)$ saturation vapour

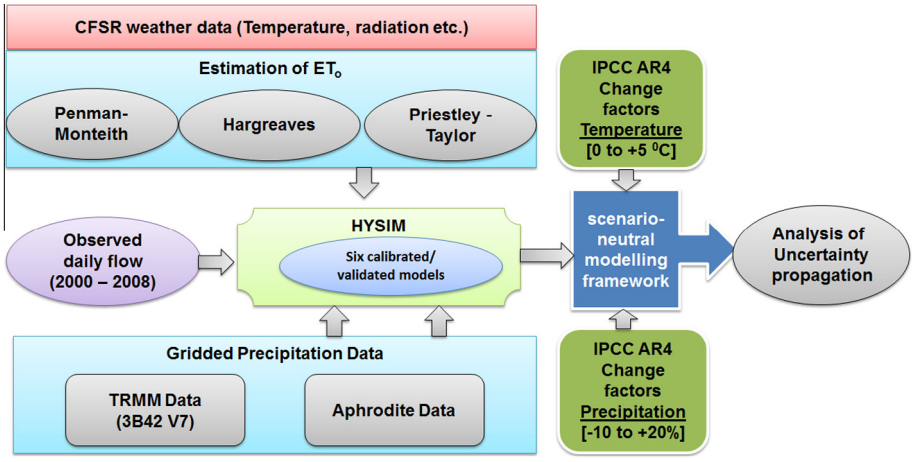


Fig. 2. Methodology adopted for analysis of uncertainty propagation in this study.

pressure deficit (kPa), Δ slope vapour pressure curve (kPa °C^{-1}), Υ psychrometric constant (kPa °C^{-1}) (Mallikarjuna et al., 2014).

2.2.2. The Hargreaves–Samani method

The Hargreaves–Samani method (Hargreaves and Samani, 1985a,b) is a well-established approach that has been shown to give similar performance to Penman–Monteith (Heydari and Heydari, 2014), but without the need for solar radiation, relative humidity and wind speed data:

$$ET_0 = 0.0135 K_{R_s} \frac{R_a}{\lambda} \sqrt{(T_{max} - T_{min})}(T + 17.8) \quad (2)$$

where R_a is the extra-terrestrial radiation (MJ m^{-2} day^{-1}), and λ is the latent heat of vaporisation (MJ kg^{-1}) for the mean air temperature T (°C), which is equal to 2.45 MJ kg^{-1}, K_{R_s} is the radiation adjustment coefficient (the numerical value is 0.17) (De Sousa Lima et al., 2013; Samani, 2004). Pandey et al. (2014) considers Hargreaves–Samani method as one of the promising approaches for estimation of reference evapotranspiration under data-scarce mountainous conditions based on experiments in East Sikkim, India.

2.2.3. The Priestley–Taylor equation

The Priestley–Taylor equation replaces the aerodynamic term in the Penman–Monteith equation with a dimensionless constant (Priestley–Taylor coefficient)

$$ET_0 = \alpha \cdot \frac{\Delta}{\Delta + \gamma} \cdot \frac{R_n - G}{HE} \quad (3)$$

where HE is specific heat of evaporation (MJ m^{-2} mm^{-1}), α Priestley–Taylor parameter (α = 1.26) and specific heat of evaporation can be calculated using HE = 0.0864 (28.9 − 0.028T) (Eidgenössische Technische Hochschule (ETH), 2014).

2.3. The HySim hydrological model

HySim is a continuous, daily conceptual rainfall–runoff model (Manley and Water Resource Associates Ltd., 2006) with separate sub-routines to simulate catchment hydrology and channel hydraulics. The catchment hydrology is simulated by seven surface and subsurface stores (snow storage, upper and lower soil horizon, transitional groundwater, groundwater storage and minor channel storage) whilst the hydraulic sub-routine uses kinematic routing of the river flows to the outlet. HySim has been extensively used in upland and mountainous catchments under current and future climate conditions (e.g. Wilby, 2005; Murphy et al., 2006).

The HySim model uses inputs of precipitation, potential evapotranspiration and temperature-based snowmelt to simulate stream flow – see Pilling and Jones (1999) for details of the main model parameters. The selection of the number of sub-catchments is subjective, but the river basin has been sub-divided on altitude, given the importance of the snow dynamics to hydrological behaviour, into Upper (permanent snow/ice), Middle (seasonal snow) and Lower (no snow) sub-catchment areas of 5720, 3440 and 3350 km^2, respectively. Areal averaging was used to change the precipitation and evapotranspiration data from the different resolution grids. HySim soil hydraulic parameters were estimated from the land uses and soil types of the region and from the literature (Jain et al., 2010; FAO/IIASA/ISRIC/ISSCAS/JRC, 2012). Initial values of the HySim soil parameters were based on the spatially-weighted physical attributes given in the Harmonized World Soil Database (HWSD) (FAO/IIASA/ISRIC/ISSCAS/JRC, 2012) [resolution of about 1 km (30 arc seconds by 30 arc seconds)] although model default values for the soil hydraulic parameters were calibrated (Schwarz, 2013). Initial rooting depths were in the range of 800 mm (grassland)–5000 mm (forest) (Manley and Water Resource Associates Ltd., 2006). Table 1 shows the minimum to maximum parameter ranges across the three sub-catchments and six HySim models, which indicates calibrated parameter variability. To characterise permanent Himalayan snow and ice cover within the simulations, the upper sub-catchment in the model was initialised with an arbitrary ice/snow depth of around 25 m informed by past research (Kulkarni et al., 2005; Kulkarni and Karyakarte, 2014; Linsbauer et al., 2014).

2.4. Model calibration and validation

HySim was independently calibrated and validated for each combination of the two global gridded data sets and the three potential evapotranspiration equations (Fig. 2), producing six validated models. After two years of model warm-up (1998–1999), each model build was calibrated using flow data for 2000–2004, and validated for 2005–2008. Seven parameters relating to land cover (rooting depth, mm (RD)); snowmelt (snow melt threshold, °C (ST); snow melt rate, mm °C^{-1} day^{-1} (SM)) and soil hydrology (Permeability of horizon boundary, mm/hour (PHB); Permeability of base lower horizon, mm/hour (PBLH); Interflow in upper layer, mm/hour (IU); and Interflow in lower layer, mm/hour (IL)) were calibrated using the commonly used Nash–Sutcliffe Efficiency Criterion (NSE – Eq. (4)) and the Percent Bias (PBIAS – Eq. (5)) goodness-of-fit measures (as recommended by Moriasi et al. 2007):

$$NSE = 1 - \frac{\sum_1^N (M_i - O_i)^2}{\sum_1^N \left(O_i - \bar{O}\right)^2} \quad (4)$$

$$PBIAS = \left[\frac{\sum_1^N (O_i - M_i) \times 100}{\sum_1^N O_i}\right] \quad (5)$$

where O_i and M_i are the observed and simulated values for the ith streamflow value, respectively, $\bar{O}$ is the mean observed value, and N is the number of days.

NSE is selected as the best objective function for reflecting the overall fit of a hydrograph (Moriasi et al., 2007) whilst PBIAS measures the average tendency of the simulated data to be larger or

Table 1
Uncertainty ranges in the HySim parameter bounds with different input space across three sub-catchments.

Parameters	TRMM Priestley–Taylor	TRMM Penman–Monteith	TRMM Hargreaves	Aphrodite Priestley–Taylor	Aphrodite Penman–Monteith	Aphrodite Hargreaves
Rooting depth (mm) (RD)	1218–2746	1121–2752	166–4285	811–1146	864–3211	2195–2766.
Permeability – horizon boundary (mm/h) (PHB)	764–7663	3.8–26	221–658	346–686	101–550	96–524
Permeability – base lower horizon (mm/hour)(PBLH)	526–529	17–163	482–711	646–777	305–569	202–377
Interflow – upper (mm/h))IU)	3.7–600	5.7–7.6	282–500	70–307	10–606	15–814
Interflow – lower (mm/h) (IL)	3015–774	82–330	78–224	103–612	18–466	24–639
Snow Threshold (°C) (ST)	0.3–2.0	0.5–0.6	1.1–1.2	2.3–2.4	1.4–2.0	1.8–2.5
Snow melt rate (mm/°C/day) (SM)	2.5–2.5	0.8–1.2	1.7–1.8	2.0–2.5	1.8–2.3	2.2–2.5

Table 2
Statistical summary of daily TRMM and APHORDITE precipitation data (1998–2007).

Indices (mm/day)	TRMM precipitation data			APHRODITE data		
	Upper sub-catchment	Middle sub-catchment	Lower sub-catchment	Upper sub-catchment	Middle sub-catchment	Lower sub-catchment
Mean	2.77	3.76	4.12	2.00	3.10	4.47
Maximum	96.44	119.44	136.83	53.74	74.07	121.18
Minimum	0.00	0.00	0.00	0.00	0.00	0.00
SD	6.69	9.00	10.04	4.50	6.85	10.66
5th percentile	0.38	0.22	0.20	0.06	0.01	0.02
95th percentile	13.83	19.28	23.19	10.02	16.14	24.38

N.B: the indices were applied on gridded average corresponding to each sub-catchment.

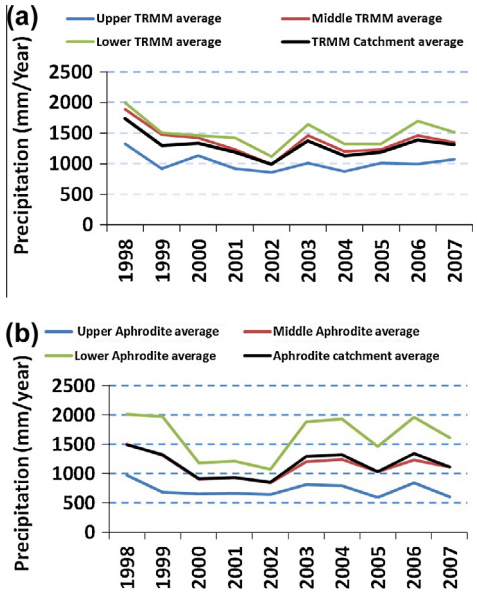


Fig. 3. Comparison of annual (a) APHRODITE and (b) TRMM precipitation data at the sub-catchment scale.

smaller than the observed data and hence quantifies overall water balance errors (Gupta et al., 1999). We have based the evaluation of model performance using these metric on the NSE and PBIAS limits specified by Moriasi et al. (2007) and Henriksen et al. (2003). For example, Moriasi et al. (2007) recommends that 'satisfactory' performance for monthly time step stream flow is given by $0.50 < NSE \leqslant 0.65$ and $\pm 15 \leqslant PBIAS\ (\%) \leqslant \pm 25$.

2.5. 'Scenario neutral method' of climate change impact assessment

Plausible ranges of future changes in annual temperature and annual precipitation were informed by the regional summary results from 25 to 39 GCMs given in Christensen et al. (2013). This study used the projections for the Tibetan Plateau area (bounded by lat. 30°–75°N and long. 50°–100°E) and the Central Asia area (lat. 30°–50°N and long.40°–75°E), as the Beas catchment is located close to the boundary of the two modelled regions. Six temperature change factors between $\Delta T = 0$ °C and $\Delta T = 5$ °C (in steps of 1 °C) and seven precipitation change factors from $\Delta P = -10\%$ to $\Delta P = +20\%$ (in steps of 5%) were used, which span the range of GCM projections for the Representative Concentration Profiles (RCP) across the two areas for 2065, and capture the median temperature increase under RCP8.5 (Riahi et al., 2011) and the 25th to 75th range in precipitation change across the RCPs to 2100. The above mentioned change factors were applied to the daily values of the whole baseline time series (2000–2008) to construct the future scenario-neutral climate variables. In

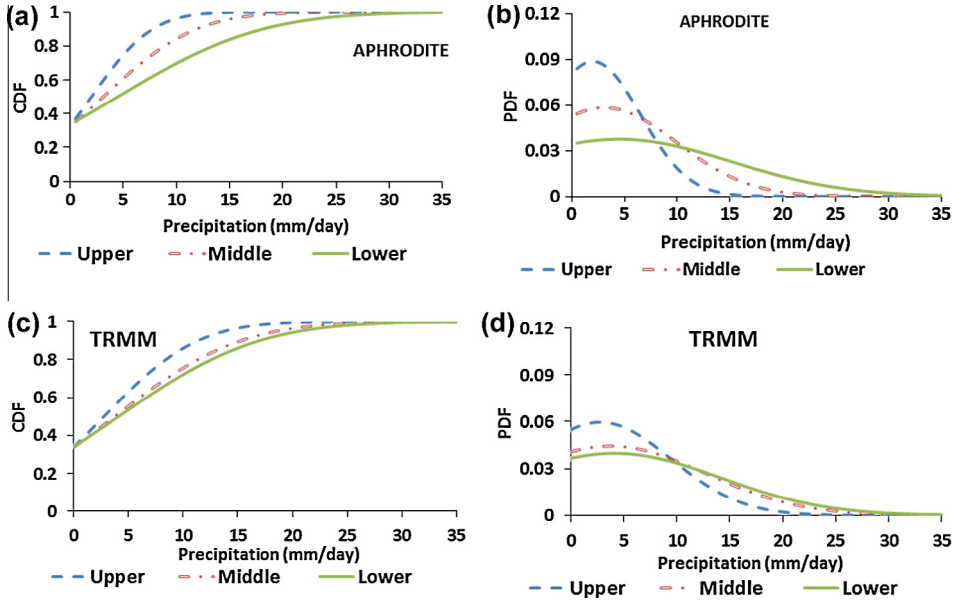


Fig. 4. Cumulative and probability density functions showing the uncertainty in the gridded precipitation datasets [TRMM and APHRODITE] in the three sub-catchments for 1998–2007 data.

the results section, all model results are compared to those from 2000 to 2008 (i.e. with zero temperature/precipitation change).

Each temperature change factor was added to the historical NCEP data to provide modified temperature and subsequently ETo time series. All other weather variables were assumed unchanged in the derivation of the modified ETo time series. The relative changes in precipitation were applied to each of the TRMM and APHRODITE historical time series (Prudhomme et al., 2010). Each of the six calibrated/validated HySim models was run for the thirty combinations of changed temperature (5) and precipitation (6). All calibrated model parameters were unchanged.

3. Results and discussions

The presentation of results is laid out as follows. Sections 3.1 and 3.2 discuss, compare and contrast the different gridded precipitation data and ETo series in three sub-catchments of the river Beas. Section 3.3 presents the HySim based model calibration and validation under the six data input combination; whilst Section 3.4 examines how the resultant model parameter uncertainty affects impact response surfaces of future Q10 and Q90 daily discharge to changes in temperature and precipitation.

Table 3
Statistical summary of daily calculated ETo (1998–2007).

Indices (mm/day)	Upper sub catchment			Middle sub catchment			Lower sub catchment		
	Penman ETo (mm)	Hargreaves ETo (mm)	Priestley–Taylor ETo	Penman ETo (mm)	Hargreaves ETo (mm)	Priestley–Taylor ETo	Penman ETo (mm)	Hargreaves ETo (mm)	Priestley–Taylor ETo
Mean	1.97	1.58	2.49	4.62	3.22	3.36	6.58	4.43	3.51
Maximum	6.31	4.47	6.43	9.70	6.79	6.75	15.92	8.84	7.21
Minimum	0.27	0.00	0.48	0.53	0.50	0.61	0.73	0.67	0.50
Standard deviation	1.03	0.96	1.38	1.80	1.44	1.85	2.65	1.91	1.99
5th percentile	1.79	1.55	2.26	4.40	3.22	3.30	6.23	4.39	3.41
95th percentile	3.87	3.19	5.05	7.94	5.50	6.16	11.36	7.50	6.42

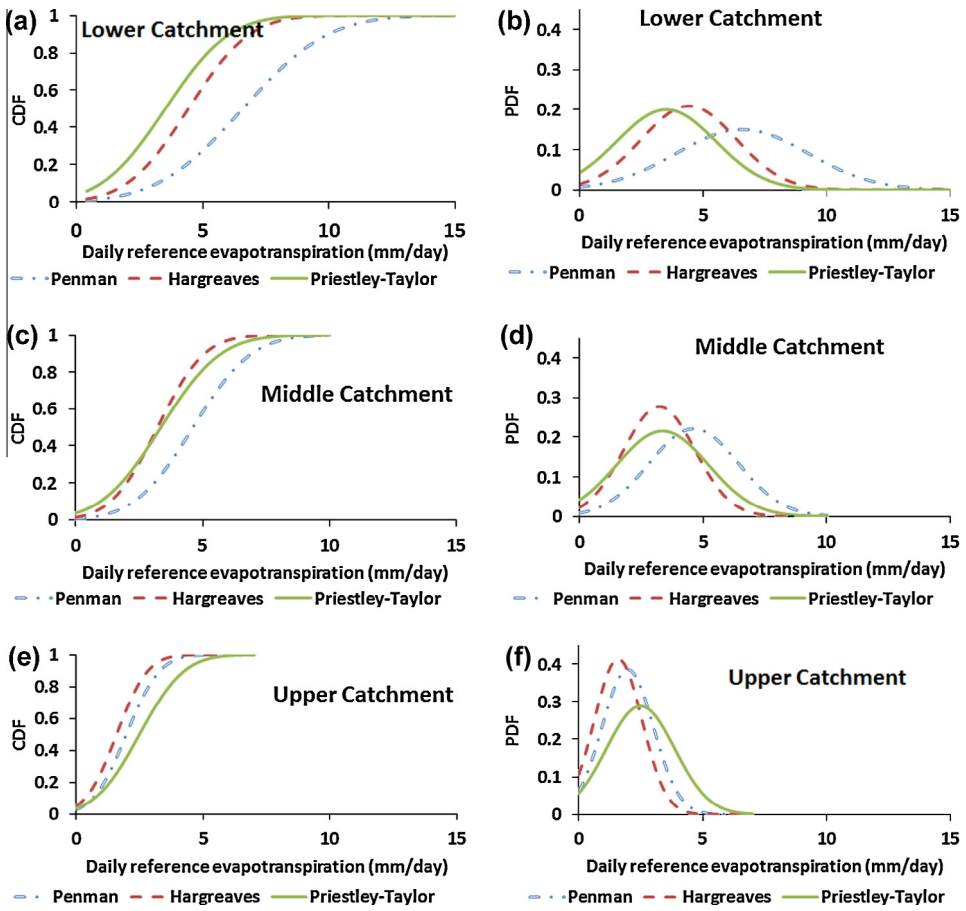


Fig. 5. Cumulative and Probability Density Functions showing the uncertainty in the different daily reference evapotranspiration time series [Penman–Monteith, Priestley–Taylor, Hargreaves–Samani] in the three sub-catchments for 1998–2007 data.

3.1. Comparison of precipitation data sets

Given the paucity of land based measurements of precipitation in the Himalayan region and the challenges of assessing the relative performance of raingauge and radar datasets (Vasiloff et al., 2009), the differences between TRMM and APHRODITE are compared (Fig. 3), but assessing their accuracy and reliability is not within the scope of this paper.

There are significant differences in the spatial and temporal distribution of precipitation between the two datasets (Table 2 and Fig. 3). Differences in average precipitation between TRMM3 B42 V7 and APHRODITE increase with increasing sub-catchment elevation. Although there is an 11% difference in annual average precipitation for the whole catchment, there is an ~39% difference in the Upper sub-catchment and ~13% in the Lower sub-catchment. The datasets have greatest monthly differences in winter (maximum difference of ~46%) and spring (maximum of ~47%) in the Upper sub-catchment; whereas the highest differences in the Lower sub-catchment are in the low flow autumn season (maximum value ~50%). In the Middle sub-catchment, the differences were in the range of ~6% (October) to ~29% (April) with the lower and higher values just after and before the South west summer Monsoon. The lowest monthly differences between the datasets in all three sub-catchments of 2–6% occurred in the summer season. The differences between the Probability Density Function (PDF) and Cumulative Density Function (CDF) plots for the TRMM and APHRODITE gridded precipitation data sets in Fig. 4 show the uncertainty in daily precipitation in the upper, middle and lower sub-catchments.

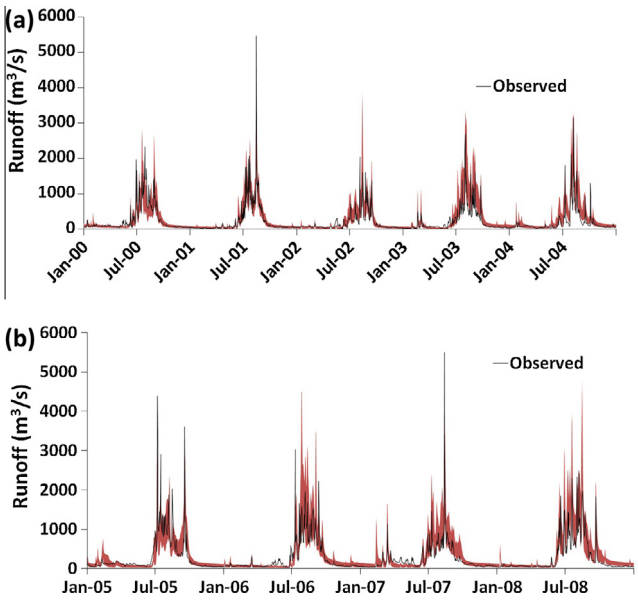


Fig. 6. The uncertainty bounds in simulated daily discharge during (upper) calibration and (lower) validation periods due to the variability in input parameter space across the six HySim models.

3.2. Comparison of reference evapotranspiration methods

As would be expected, all three ETo methods give decreasing ETo with increasing sub-catchment elevation (Table 3). However, there are distinct differences between the methods with Penman–Monteith giving annual average values that are 47% and 30% higher than the methods giving the lowest values in the Lower (Priestley Taylor) and Middle (Hargreaves–Samani) sub-catchments. In contrast, the Priestley–Taylor method gave the highest annual average value in the Upper glacier dominated sub-catchment, which was 36% higher than the lowest method (Hargreaves). The PDFs and CDFs of daily reference evapotranspiration for 2000–2008 used to drive the six hydrological models, given in Fig. 5, demonstrate the significant uncertainty introduced by the choice of ETo method (Priestly–Taylor, Penman–Monteith, and Hargreaves–Samani).

3.3. Hydrological modelling – calibration and validation

Fig. 6 shows the narrow uncertainty bounds in simulated daily flow across the six models for both the calibration and validation periods. The strong seasonality in observed river response associated with the monsoon and snow melt is reproduced. There is generally good agreement across the flow duration curve (Fig. 1 of the Supplementary material), with the six models spanning the observed flows through the flow range, with the exception of about the upper 5% exceedance probability which may partly reflect the difficulty of accurately measuring such high discharges.

Similar levels of model performance were achieved across the 6 model combinations in the calibration period, with NSE varying between 0.64 and 0.70. The three TRMM models having slightly higher NSEs and lower PBIAS (Table 4). The performance metrics for the three TRMM models are very similar in the validation phase (0.66–0.71), although there is an increase in the PBIAS. In contrast,

Table 4
Statistical indices of HySim model performance for different precipitation and evapotranspiration combinations.

Calibration (2000–2004)							Validation (2005–2008)					
Year	Penman–Monteith		Priestley–Taylor		Hargreaves		Year	Penman–Monteith		Priestley–Taylor		Hargreaves	
	PBIAS (%)	NSE	PBIAS (%)	NSE	PBIAS (%)	NSE		PBIAS (%)	NSE	PBIAS (%)	NSE	PBIAS (%)	NSE (%)
TRMM precipitation data with different ETo combinations													
2000	16.8	0.75	4.3	0.75	10.9	0.74	2005	39.9	0.50	31.7	0.57	31.8	0.66
2001	20.9	0.69	17.3	0.73	16.5	0.70	2006	31.2	0.70	21.5	0.75	26.9	0.70
2002	11.9	0.59	4.6	0.55	−3.3	0.53	2007	14.6	0.72	2.3	0.69	7.2	0.71
2003	1.5	0.77	−9.9	0.75	−10.4	0.71	2008	−2.4	0.74	−14.9	0.71	−7.1	0.77
2004	0.5	0.69	−11.8	0.68	−13.3	0.65	Average	20.8	0.66	10.2	0.68	14.7	0.71
Average	7.54	0.70	4.1	0.69	3.5	0.67							
APHRODITE precipitation data with different ETo combinations													
2000	28.2	0.60	34.4	0.54	36.8	0.57	2005	25.1	0.56	24.8	0.51	30.8	0.54
2001	18.1	0.69	26.4	0.67	21.6	0.68	2006	−0.6	0.44	−1.5	0.46	7.1	0.39
2002	0.5	0.69	14.9	0.74	5.3	0.66	2007	0.4	0.44	1.5	0.45	8.5	0.46
2003	−19.7	0.69	−14.0	0.75	−15.5	0.64	2008	−14.6	0.72	−14.0	0.77	−17.5	0.73
2004	−36.7	0.62	−29.1	0.70	−27.1	0.62	Average	2.58	0.54	2.69	0.55	7.24	0.53
Average	6.80	0.66	6.51	0.68	12.02	0.64							

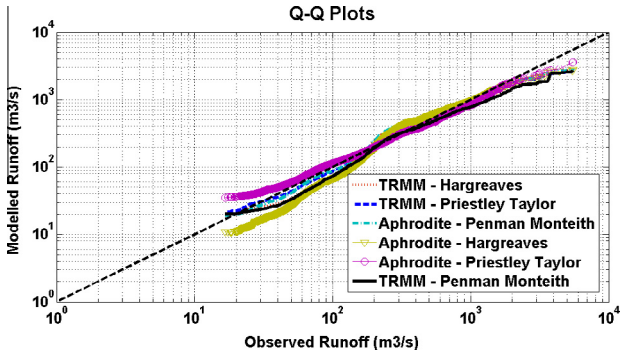


Fig. 7. Q–Q plot evaluation of the modelled daily discharge in the six models against observed discharge data for 2000–2008.

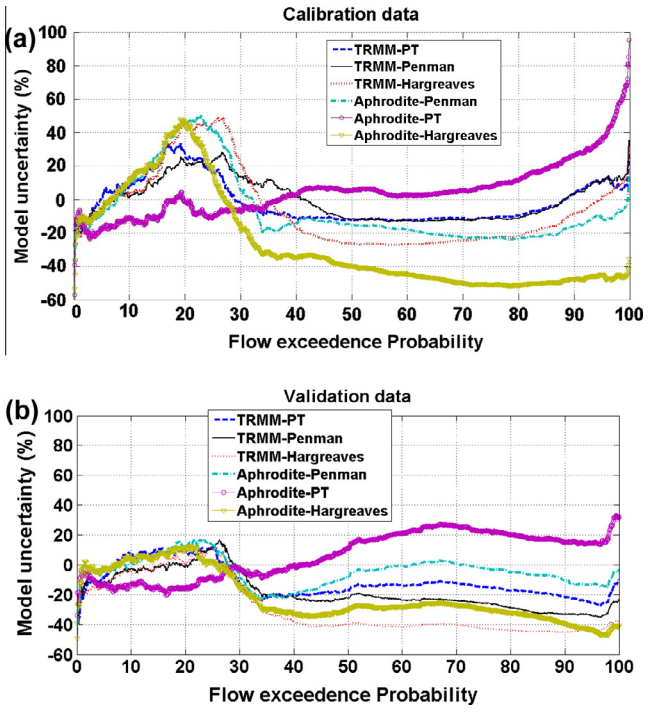


Fig. 8. (a–b) Model uncertainty (as given by the percentage difference between simulated and observed discharge) along the flow exceedance curves showing associated uncertainties in six hydrological modelling setups under the calibration (2000–2004) and validation (2005–2008) phases.

the NSE for the APHOPRITE runs within the validation period reduce (0.53–0.55), albeit still within the satisfactory range as defined by Moriasi et al. (2007) and Henriksen et al. (2003), but is accompanied by an improvement in the PBIAS to 2.6–7.2%. The reliability of the predictive output distribution in the different models is demonstrated using the quantile–quantile (Q–Q) plots in Fig. 8. Although the overall performances of the models (as given by the NSE and PBIAS metrics for the calibration and validation periods) are similar, it is apparent from Fig. 7 that there are parameter-related uncertainties in simulated discharge. Fig. 8(a and b) express this uncertainty by showing the model uncertainty (as given by the percentage difference between simulated and observed discharge) associated with flow exceedance probability for each of the models during the calibration (2000–2004) and validation (2005–2008) periods. The discharge uncertainty arising from the model parameterisations are from +8% to −13% for Q10 and +15% to −45% for Q90 in the validation period.

Table 1 shows that the variability in the observational input data space has led to quite different optimal parameter vectors with similar model performance The differences in the performance metrics and calibrated parameter values across the six models solely reflect the effects of the differences in the input precipitation and ETo data, given that all other input data and the observed discharge data are consistent across the six models. This demonstrates how the calibration process can effectively modify hydrological parameters to compensate for uncertainties in input data.

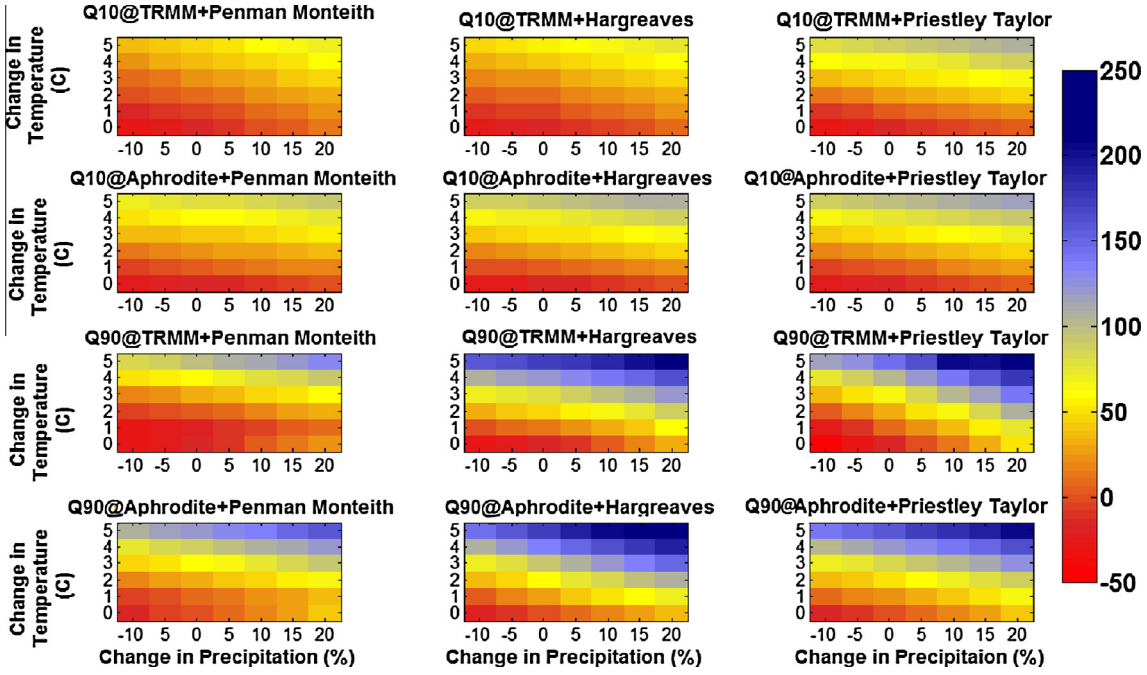


Fig. 9. Impact response surfaces of simulated changes (%) in (upper) Q10 and (lower) Q90 to changes in annual precipitation and temperature for the six HySim models.

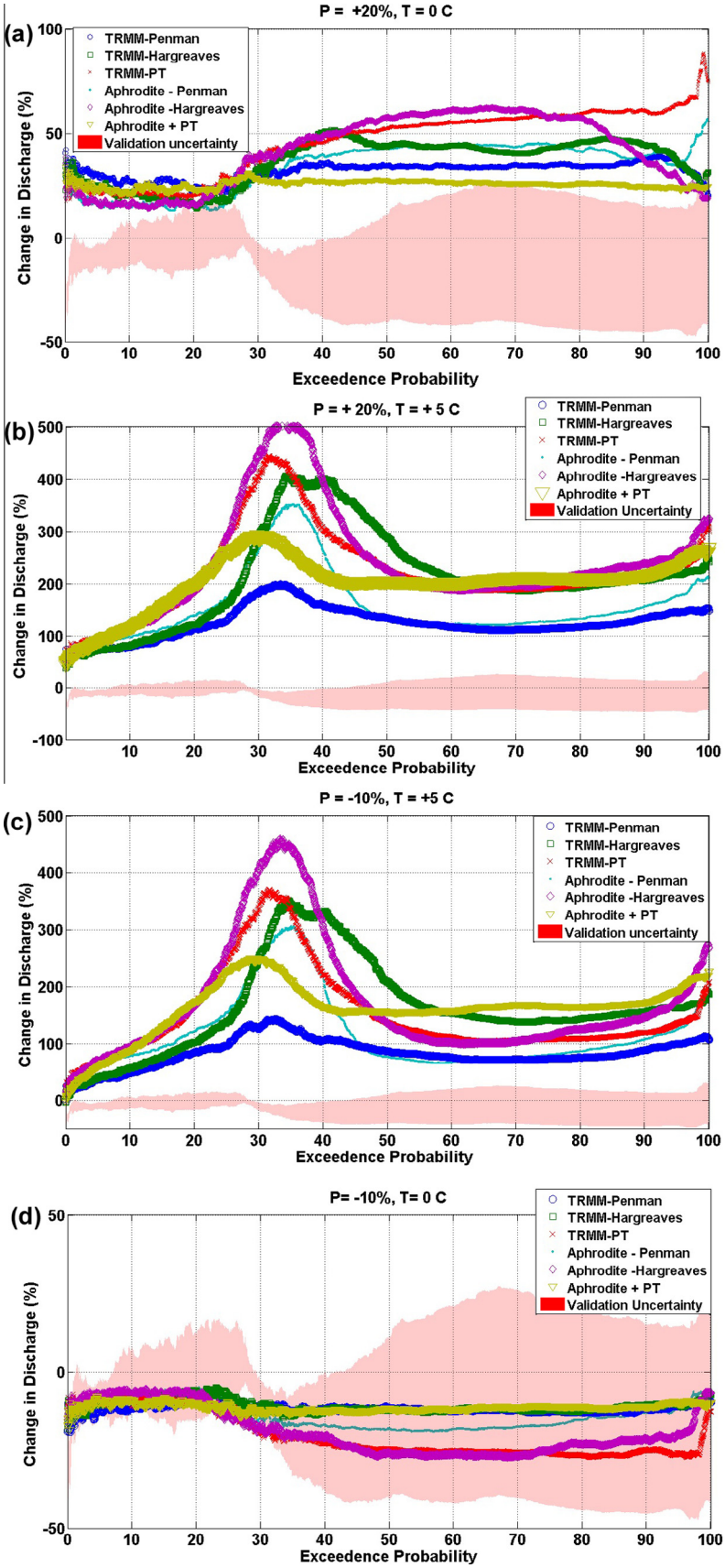


Fig. 10. Comparison of the model validation uncertainty (grey shaded area) with the future impact uncertainty (as given by the spread of the percentage change in future daily discharge relative to the baseline for the 6 HySim models) across the flow exceedance probability for four change factor scenarios showing how the spread of future hydrological uncertainty expands from the uncertainty due to the input data selection subjectivity impacts validation period as the change in climate increases.

3.4. Effect of parameter uncertainty on climate change impact response surfaces

The daily flow that is equalled or exceeded 10 and 90% of the time (annual high flow (Q10) and annual low flow (Q90)), respectively, are commonly used in designing hydropower projects (IITR, 2011). Fig. 9 shows the impact response surfaces for each of the 6 validated models for Q10 and Q90, expressed as a percentage of that model's baseline (2000–2008) value, across the range of plausible changes in future annual temperature and precipitation. The uncertainty range in Q10 and Q90 across the six different models is given in Fig. 2 of the Supplementary material. Both flow indices generally change in proportion to the changes in both precipitation and temperature, indicating that the increases in temperature produce greater modelled increases in snowmelt than actual evapotranspiration. The simulated median (Q50), annual high flow index (Q10) and annual low flow index (Q90) characterising the hydrological impacts of plausible climate change as simulated by the six HySim models are given in Table 1 of the Supplementary material. This indicates that the differences in hydrological parameters arising from input uncertainty have greater impact on the uncertainties in low flows (Q90) than on high flows (Q10).

The Q90 is more sensitive to precipitation and temperature changes than the Q10 in relative terms, as a given absolute change in flow represents a larger proportion for low flows than high flows. The greatest decrease in both metrics occurs under the (ΔT = 0 °C – ΔP = −10%) scenario, ranging from −25% (TRMM-Priestley–Taylor) to −2% (TRMM + Penman–Monteith) for Q90; and from −11% (TRMM + Penman–Monteith) to −6%, (APHRODITE + Penman–Monteith) for Q10.

Similarly, the greatest increases occurred under the (ΔT = +5 °C – ΔP = +20%) scenario due to the increased precipitation and snowmelt outweighing the effects of increased evaporation/evapotranspiration – they ranged from +133% (TRMM + Penman–Monteith) to 238% (APHRODITE – Hargreaves) for Q90, representing an absolute increase in the Q90 flow of between 37–51 m^3/s; and from +79% (TRMM + Penman–Monteith) to +118% (APHRODITE – Priestley–Taylor) for Q10 equivalent to a modelled increase of 470–771 m^3/s. It is apparent that, whilst the general trends in the response surfaces for the 6 different models respond similarly across temperature and precipitation changes, the choice of precipitation dataset and ETo method differentially affects the magnitude of changes in Q90 and Q10. Fig. 10 shows how the parameter differences associated with the choice of baseline data impact on the flow duration curves for selected future climate scenarios, superimposed with the uncertainty range for the 6 models for the validation period (from Fig. 8b). The selected scenarios are [ΔP = −10%, ΔT = 0 °C] (highest reduction in precipitation and no change in temperature), [ΔP = −10%, ΔT = 5 °C] (highest reduction in precipitation and highest change in temperature), [ΔP = +20%, ΔT = 0 °C] (highest increase in precipitation and no change in temperature), [ΔP = +20%, ΔT = 5 °C] (highest increase in precipitation and temperature from baseline climate). These show that large precipitation changes in the absence of temperature increases tend to lead to the largest percentage changes in the median to low flow end of the flow duration curve; whereas temperature increases cause the largest increase around the 25th to 50th exceedance probability reflecting large increases in pre- and post-monsoon snowmelt. However, when the future discharge uncertainty for the 6 models across the range of flow exceedance is compared with the model uncertainty from the validation period, it is apparent that the future changes in discharge tend to exceed the validation uncertainty across the flow exceedance range, with the exception of small climate changes (e.g. [ΔP = −10%, ΔT = 0 °C]). Decreasing precipitation decreases the uncertainty range but temperature increases have a much greater impact on the uncertainty. It is apparent that, in the case of such a highly responsive snow-dominated catchment, stream flow uncertainty is smaller with changes in precipitation than that of temperature. For the [Aphrodite + Penman–Monteith] model, a hydrological uncertainty range of −6.4% to 16% was associated with changes in precipitation from −10% to +20% at ΔT = 0, compared to an uncertainty range of 0 to +84% for temperatures change of 0 to +5 °C at ΔP = 0%.

4. Discussion and conclusion

The need to understand uncertainty within water resource assessments is widely recognised (Refsgaard et al., 2007), and many elements of the uncertainty cascade within climate impacts modelling have been quantitatively assessed, highlighting the relative importance of GCM choice, emissions scenario, downscaling method, model choice, etc. (Pappenberger and Beven, 2006; Buytaert et al., 2009; Kay et al., 2009; Chen et al., 2011). However, the role of modeller subjectivity is generally ignored, despite its recognition in other modelling fields, such as pesticide fate (Dubus et al., 2003; Beulke et al., 2006) and hydraulic modelling (Garcia-Salas and Chocat, 2006).

In this paper, we have investigated the combined consequence of modeller choice on two key elements of a hydrological model build in data-sparse areas which, to-date, have received little consideration in the context of their overall contribution to the uncertainty in climate impact assessment – the choice of baseline precipitation dataset and the choice of method for deriving reference evapo-transpiration.

The consequence of the differing model parameterisations resulting from the dataset/method choice in this study, through calibrating the hydrological model with different precipitation and ETo time series, do not manifest themselves in significant differences in model behaviour and performance during the historical baseline period as given by conventional performance metrics. The HySim model was demonstrated to have similar NSE and PBIAS values and flow duration curves to the observed river flows across the 6 model builds, despite the significant uncertainty in daily precipitation between APHRODITE and TRMM and notwithstanding issues around the use of such data products in daily hydrological modelling (Zhao et al., 2013; Meng et al., 2014). The similar model performance reflects the 'success' of each of the calibrations in modifying the parameter values which control the rates and thresholds of hydrological processes to compensate for differences in precipitation and ETo amount (through changing snow melt characteristics and the actual ET via the rooting depth) and timing (through changing the rates of vertical and horizontal flow through the sub-catchments) to enable the simulated river flows to satisfactorily match the observed. The results demonstrate that uncertainty in any set of hydrologic inputs (here precipitation and evapotranspiration) can be conserved, with the translation of this uncertainty into simulated stream flow and performance metrics concealed or reduced through the calibration of model parameters (Singh and Bárdossy, 2012, Andreassian et al., 2004 and Oudin et al. 2006). However, parameter-related uncertainties do exist in the baseline simulated discharge, as shown by the range of discharge error within the 6 models along the flow exceedance curves (Fig. 8).

It is usual for modellers to assume that the range of uncertainty and model performance statistics assessed during calibration and validation remain largely invariant, regardless of the type or source of input data sets used for modelling (McMillan et al., 2011). However, our analysis has shown that the baseline uncertainty due to parameter bias (Fig. 8) is generally exceeded by the uncertainty associated with applying those models with altered climate (indicating that model uncertainty is not invariant) and that the impact uncertainty (arising from model parameterisation) magnifies as the difference from the current climate increases (Fig. 10).

This study has highlighted that the use of state-of-art techniques for parameter estimation can still allow parameter bias, given the input space used for calibration. The consequence of such concealed uncertainty and parameter bias rematerialize in climate change impact studies when models are taken outside of the input space of the calibration/validation period.

This paper has used a simple scenario-neutral framework to illustrate the important consequences of model calibration with alternative meteorological time series data for assessing climate change impacts. We acknowledge the simplification in assuming that future ETo is only modified by changing temperature, whilst assuming other meteorological variables such as solar radiation and wind velocity which may also influence future evapotranspiration dynamics remain unchanged). However, the insights are pertinent to more sophisticated climate change impacts approaches where hydrological models are calibrated to observed flows using imperfect baseline meteorological data.

Refsgaard et al. (2007) state that uncertainty assessment is not something to be added after the completion of the modelling work, but should be seen as running throughout the modelling study starting from the very beginning. This paper supports this assertion, and demonstrates that input data choices made by a modeller prior to the model build influence the behaviour and results of the calibrated model when run with perturbed weather inputs. Whilst the uncertainty range across the scenario-neutral modelling space due to the choice of precipitation product and ETo method (of up to 105% and 39% of the simulated baseline Q90 and Q10 values, respectively) is smaller than the widely acknowledge effects of GCM uncertainty on flows (e.g. Buytaert et al., 2009), the difficulties of measuring precipitation and ETo amount and timing in mountainous regions will remain. Modellers must therefore be aware of the implications of their choice of baseline data for the simulation of future impacts. In such conditions where there is considerable uncertainty in observed meteorological data and/or different satellite based precipitation and temperature data products are available, an ensemble of hydrological model-builds calibrated to the different combinations of available meteorological forcing data should be used to inform the understanding of the uncertainties associated with input selection and the resultant effect of parameter biases on climate change impact studies.

This study has provided the first quantitative evaluation of how the recognised compensation-effect of hydrological model parameterization for input data uncertainty affects the magnitude of future simulated climate change impacts. The recognition of how the subjectivity of the hydrological modeller in input selection choices can influence impact results, and that the range of baseline model uncertainty is not conserved within future impacts, has important implications for future climate change impact and adaptation studies, especially in data-sparse regions.

Acknowledgements

Special thanks are extended to Dr Sanjay Jain (National Institute of Hydrology, Roorkee) and Bhakra Beas Management Board for supplying discharge data. Water Resource Associates are thanked for the use of the HySim software. This work was supported by the Natural Environment Research Council (NERC) – United Kingdom (grant number NE/I022329/1), as part of a joint NERC – Indian Ministry of Earth Sciences research programme. The HySim model outputs can be accessed by contacting research-data@cranfield.ac.uk.

Appendix A. Supplementary material

Supplementary data associated with this article can be found, in the online version, at http://dx.doi.org/10.1016/j.jhydrol.2015.06.026.

References

Allen, R.G., Pereira, L.S., Raes, D., Smith, M., 1998. Crop Evapotranspiration – Guidelines for Computing Crop Water Requirements, FAO Irrigation and Drainage Paper 56. Food and Agriculture Organization of the United Nations, Rome.

Andermann, C., Bonnet, S., Crave, A., Davy, P., Longuevergne, L., Gloaguen, R., 2012. Sediment transfer and the hydrological cycle of Himalayan rivers in Nepal. C.R. Geosci. 344 (11–12), 627–635.

Andermann, C., Bonnet, S., Gloaguen, R., 2011. Evaluation of precipitation data sets along the Himalayan front. Geochem. Geophys. Geosyst. 12, Q07023. http://dx.doi.org/10.1029/2011GC003513.

Andreassian, V., Perrin, C., Michel, C., 2004. Impact of imperfect potential evapotranspiration knowledge on the efficiency and parameters of watershed models. J. Hydrol. 286, 19–35.

Baldocchi, D., Falge, E., Gu, L., et al., 2001. FLUXNET: a new tool to study the temporal and spatial variability of ecosystem-scale carbon dioxide, water vapor, and energy flux densities. Bull. Am. Meteorol. Soc. 82 (11), 2415–2434.

Beulke, S., Brown, C.D., Dubus, I.G., Galicia, H., Jarvis, N., Schaefer, D., Trevisan, M., 2006. User subjectivity in Monte Carlo modeling of pesticide exposure. Environ. Toxicol. Chem. 25 (8), 2227–2236.

Buytaert, W., Célleri, R., Timbe, L., 2009. Predicting climate change impacts on water resources in the tropical Andes: effects of GCM uncertainty. Geophys. Res. Lett. 36, L07406. http://dx.doi.org/10.1029/2008GL037048.

Chen, J., Brissette, P.F., Leconte, R., 2011. Uncertainty of downscaling method in quantifying the impact of climate change on hydrology. J. Hydrol. 401 (3–4), 190–202. http://dx.doi.org/10.1016/j.jhydrol.2011.02.020.

Christensen, J.H., Krishna Kumar, K., Aldria, E., An, S.-I., Cavalcanti, I.F.A., de Castro, M., Dong, W., Goswami, P., Hall, A., Kanyanga, J.K., Kitoh, A., Kossin, J., Lau, N.- C., Renwick, J., Stephenson, D.B., Xie, S.-P., Zhou, T., 2013. Climate phenomena and their relevance for future regional climate change supplementary material. In: Stocker, T.F., D. Qin, G.-K. Plattner, M. Tignor, S.K. Allen, J. Boschung, A. Nauels, Y. Xia, V. Bex., P.M. Midgley (Eds.), Climate Change 2013: The Physical Science Basis. Contribution of Working Group I to the Fifth Assessment Report of the Intergovernmental Panel on Climate Change. <http://www.climatechange2013.org and www.ipcc.ch>.

Collischonn, B., Collischonn, W., Tucci, C.E.M., 2008. Daily hydrological modeling in the Amazon basin using TRMM rainfall estimates. J. Hydrol. 360 (1–4), 207–216. http://dx.doi.org/10.1016/j.jhydrol.2008.07.032.

Collischonn, B., Allasia, D., Collischonn, W., Tucci, C.E.M., 2007. Performance of TRMM satellite precipitation estimates over the Upper Paraguai River Basin. Revista Brasileira de Cartografia 59 (01), 93–97.

De Sousa Lima et al., 2013. Calibration of Hargreaves–Samani equation for estimating reference evapotranspiration in sub-humid region of Brazil. J. Water Resour. Prot. 5 (12A), 1–5. http://dx.doi.org/10.4236/jwarp.2013.512A001.

Dubus, I.G., Brown, C.D., Beulke, S., 2003. Sources of uncertainty in pesticide fate modelling. Sci Total Environ. 317 (1–3), 53–72.

Eidgenössische Technische Hochschule (ETH), 2014. Empirical evapotranspiration models. <http://www.luiw.ethz.ch/labor2/experimente/exp4/Presentation/Empirical_ET_Models> (downloaded on 14.10.14).

FAO/IIASA/ISRIC/ISSCAS/JRC, 2012. Harmonized World Soil Database (version 1.2). FAO, Rome, Italy and IIASA, Luxemburg, Austria. <http://webarchive.iiasa.ac.at/Research/LUC/External-World-soil-database/HTML/index.html>.

Fowler, H., Kilsby, C., 2007. Using regional climate model data to simulate historical and future river flows in northwest England. Clim. Change 80 (3), 337–367. http://dx.doi.org/10.1007/s10584-006-9117-3.

Garcia-Salas, J.C., Chocat, B., 2006. Assessment of uncertainties in the modelling of CSOs. Water Sci. Technol. 54 (6–7), 247–254.

Gupta, H.V., Sorooshian, S., Yapo, P.O., 1999. Status of automatic calibration for hydrologic models: comparison with multilevel expert calibration. J. Hydrol. Eng. 4 (2), 135–143.

Habib, E., Henschke, A., Adler, R., 2009. Evaluation of TMPA satellite-based research and real-time rainfall estimates during six tropical-related heavy rainfall events over Louisiana, USA. Atmos. Res. 94, 373–388.

Hargreaves, G.H., Samani, Z.A., 1985a. Reference crop evapotranspiration from temperature. Appl. Eng. Agric. 1, 96–99.

Hargreaves, G.H., Samani, Z.A., 1985b. Reference crop evapotranspiration from ambient air temperature. In: Proceedings of the Winter Meeting of the American Society of Agricultural Engineers, Paper No. 85-2517, Chicago, Ill, USA, December 1985.

Heydari, M.M., Heydari, M., 2014. Calibration of Hargreaves–Samani equation for estimating reference evapotranspiration in semiarid and arid regions. Arch. Agron. nd Soil Sci. 60 (5), 695–713. http://dx.doi.org/10.1080/03650340.2013.808740.

Henriksen, H.J., Troldborg, L., Nyegaard, P., Sonnenborg, T.O., Refsgaard, J.C., Madsen, B., 2003. Methodology for construction, calibration and validation of a national hydrological model for Denmark. J. Hydrol. 280 (1–4), 52–71.
Indian Insitute of Technology Roorke (IITR), 2011. General – Project Hydrology and Installed Capacity. Standards/Manuals/Guidelines for small hydro development. Alternate Hydro Energy Center, India.
Jain, S.K., Tyagi, J., Singh, V., 2010. Simulation of runoff and sediment yield for a himalayan watershed using SWAT model. J. Water Resour. Prot. 2, 267–281.
Jain, S.K., Agarwal, P.K., Singh, V.P., 2007. Hydrology and Water Resources of India. Springer, The Netherlands.
Jamandre, C.A., Narisma, G.T., 2013. Spatio-temporal validation of satellite-based rainfall estimates in the Philippines. Atmos. Res. 122, 599–608.
Kay, A.L., Davies, H.N., 2008. Calculating potential evaporation from climate model data: a source of uncertainty for hydrological climate change impacts. J. Hydrol. 358, 221–239.
Kay, A.L., Davies, H.N., Bell, V.A., Jones, R.G., 2009. Comparison of uncertainty sources for climate change impacts: flood frequency in England. Clim. Change 92, 41–63.
Kulkarni, A.V., Karyakarte, Y., 2014. Observed changes in Himalayan glaciers. Curr. Sci. 106 (2), 237–244.
Kulkarni, A.V., Rathore, B.P., Mahajan, S., Mathur, P., 2005. Alarming retreat of Parbati glacier, Beas, Himachal Pradesh. Curr. Sci. 88 (11), 1844–1850.
Kumar, R., Shankar, V., Kumar, M., 2011. Modelling of crop reference evapotranspiration: a review. Univ. J. Environ. Res. Technol. 1 (3), 239–246.
Kumar, R., Jat, M.K., Shankar, V., 2012. Methods to estimate irrigated reference crop evapotranspiration – a review. Water Sci. Technol. 66 (3), 525–535. http://dx.doi.org/10.2166/wst.2012.191.
Legates, D.R., Willmott, C.J., 1990. Mean seasonal and spatial variability in gauge-corrected, global precipitation. Int. J. Climatol. 10 (2), 111–127.
Li, X.H., Zhang, Q., Xu, C.Y., 2012. Suitability of the TRMM satellite rainfalls in driving distributed hydrological model for water balance computations in Xinjiang catchment, Poyang lake basin. J. Hydrol. 426, 28–38.
Linsbauer, A., Frey, H., Haeberli, W., Machguth, H., 2014. Modelling Bed Overdeepenings for the Glaciers in the Himalaya-Karakoram Region Using GlabTop2. <http://www.eclim-research.ch/data/ihcap/2014egu_HimalayaKarakoram_overdeepenings.pdf> (downloaded on 15.10.14).
Lu, L., Cosmo, S.N., Xu, C.-Y., Gong, L., 2013. Comparison of the global TRMM and WFD precipitation datasets in driving a large-scale hydrological model in southern Africa. Hydrol. Res. 44 (5), 770–788.
Mallikarjuna, P., Jyothy, S.A., Murthy, D.S., Reddy, K.C., 2014. Performance of recalibrated equations for the estimation of daily reference evapotranspiration. Water Resour. Manage 28 (13), 4513–4535.
Manley R.E., Water Resource Associates Ltd., 2006. A Guide to Using HySim. Version HySim 4.90.
Maurer, E.P., 2007. Uncertainty in hydrologic impacts of climate change in the Sierra Nevada, California, under two emissions scenarios. Clim. Change 82, 309–325. http://dx.doi.org/10.1007/s10584-006-9180-9.
McMillan, H., Jackson, B., Clark, M., Kavetski, D., Woods, R., 2011. Rainfall uncertainty in hydrological modelling: an evaluation of multiplicative error models. J. Hydrol. 400 (1–2), 83–94.
Meng, J., Li, L., Hao, Z., Wang, J., Shao, Q., 2014. Suitability of TRMM satellite rainfall in driving a distributed hydrological model in the source region of Yellow River. J. Hydrol. 509 (13), 320–332.
Moriasi, D.N., Arnold, J.G., Van Liew, M.W., Bingner, R.L., Harmel, R.D., Veith, T.L., 2007. Model evaluation guidelines for systematic quantification of accuracy in watershed simulations. Tran. ASABE 50 (3), 885–900.
Mueller, B. et al., 2011. Evaluation of global observations-based evapotranspiration datasets and IPCCAR4 simulations. Geophys. Res. Lett. 38, L06402. http://dx.doi.org/10.1029/2010GL046230.
Mueller, B., Hirschi, M., Jimenez, C., Ciais, P., Dirmeyer, P.A., Dolman, A.J., Fisher, J.B., Jung, M., Ludwig, F., Maignan, F., Miralles, D.G., McCabe, M.F., Reichstein, M., Sheffield, J., Wang, K., Wood, E.F., Zhang, Y., Seneviratne, S.I., 2013. Benchmark products for land evapotranspiration: LandFlux-EVAL multi-data set synthesis. Hydrol. Earth Syst. Sci. 17, 3707–3720. http://dx.doi.org/10.5194/hess-17-3707-2013.
Murphy, C., Fealy, R., Charlton, R., Sweeney, J.S., 2006. The reliability of an "off the shelf" conceptual rainfall–runoff model for use in climate impact assessment: uncertainty quantification using Latin hypercube sampling. Area 38 (1), 65–78.
Ngongondo, C., Xu, C.-Y., Tallaksen, L.M., Alemaw, (in press). Evaluation of the FAO Penman–Monteith, Priestley–Taylor and Hargreaves models for estimating reference evapotranspiration in southern Malawi. Hydrol. Res. http://dx.doi.org/10.2166/nh.2012.224.
Oudin, L., Perrin, C., Mathevet, T., Andreassian, V., Michel, C., 2006. Impact of biased and randomly corrupted inputs on the efficiency and the parameters of watershed models. J. Hydrol. 320, 62–83.
Pandey, S., 2002. Status and distribution of some Caprids in Himachal Pradesh. In: Sathyakumar, S. Bhatnagar, Y.V. (Eds.), ENVIS Bulletin: Wildlife and Protected Areas, pp. 30–33.
Pandey, V., Pandey, P.K., Mahanta, A.P., 2014. Calibration and performance verification of Hargreaves Samani equation in a humid region. Irrig. Drain. 63, 659–667. http://dx.doi.org/10.1002/ird.1874.
Pappenberger, F., Beven, K.J., 2006. Ignorance is bliss: or seven reasons not to use uncertainty analysis. Water Resour. Res. 42, W05302. http://dx.doi.org/10.1029/2005WR004820.
Pilling, C., Jones, J.A.A., 1999. High resolution climate change scenarios: implications for British runoff. Hydrol. Process. 13 (17), 2877–2895.
Priestley, C.H.B., Taylor, R.J., 1972. On the assessment of surface heat flux and evaporation using large-scale parameters'. Mon. Weather Rev. 100 (2), 81–92.
Prudhomme, C., Wilby, R.L., Crooks, S., Kay, A.L., Reynard, N.S., 2010. Scenario-neutral approach to climate change impact studies: application to flood risk. J. Hydrol. 390 (3–4), 198–209.
Riahi, K., Rao, S., Krey, V., Cho, C., Chirkov, V., Fischer, G., Kindermann, G., Nakicenovic, N., Rafaj, P., 2011. RCP8.5—a scenario of comparatively high greenhouse gas emissions. Clim. Chang 109, 33–57. http://dx.doi.org/10.1007/s10584-011-0149-y.
Refsgaard, J.C., van der Sluijs, J.P., Hojberg, A.L., Vanrollenghem, P.A., 2007. Uncertainty in the environmental modelling process – a framework and guidance. Environ. Modell. Softw. 22 (11), 1543–1556.
Samani, Z., 2004. Discussion of 'History and Evaluation of Hargreaves Evapotranspiration Equation' by George H. Hargreaves and Richard G. Allen. J. Irrig. Drain. Eng. ASCE 130 (5), 447–448. http://dx.doi.org/10.1061/(ASCE)0733-9437(2004)130:5(447.2).
Schwarz, T., 2013. Hydrological Response of Himalayan Catchments to Climate Change: Case Study of the Beas Basin, North India. Unpublished Master's Thesis. Cranfield University.
Singh, P., Bengtsson, L., 2003. Effect of warmer climate on the depletion of snow-covered area in the Satluj basin in the western Himalayan region. Hydrol. Sci. J. 48 (3), 413–425.
Singh, D., Ganju, A., 2008. Mountain range specific analog weather forecast model for northwest Himalaya in India. J. Earth Syst. Sci. 117 (5), 575–587.
Singh, S.K., Bárdossy, A., 2012. Calibration of hydrological models on hydrologically unusual events. Adv. Water Resour. 38 (81–91), 2012. http://dx.doi.org/10.1016/j.advwatres.2011.12.006.
Thompson, J.R., Green, A.J., Kingston, D.G., 2014. Potential evapotranspiration-related uncertainty in climate change impacts on river flow: an assessment for the Mekong River basin. J. Hydrol. 510, 259–279.
Tian, Y., Peters-Lidard, C.D., Choudhury, B.J., Garcia, M., 2007. Multitemporal analysis of TRMM-based satellite precipitation products for land data assimilation applications. J. Hydrometeorol. 8 (6), 1165–1183.
Vasiloff, S.V., Howard, K.W., Zhang, J., 2009. Difficulties with correcting radar rainfall estimates based on rain gauge data: a case study of severe weather in Montana on 16–17 June 2007. Weather Forecast. 24 (5), 1334–1344.
Wilby, R.L., 2005. Uncertainty in water resource model parameters used for climate change impact assessment. Hydrol. Proc. 19 (16), 3201–3219.
Wilby, R.L., Dessai, S., 2010. Robust adaptation to climate change. Weather 65 (7), 180–185.
Wilby, R.L., Charles, S.P., Zorita, E., Timbal, B., Whetton, P., Mearns, L.O., 2004. Guidelines for use of climate scenarios developed from statistical downscaling methods. Supporting Material of the Intergovernmental Panel on Climate Change, Available from the DDC of IPCC TGCIA, pp. 27.
Woldemeskel, F.M., Sharma, A., Sivakumar, B., Mehrotra, R., 2012. An error estimation method for precipitation and temperature projections for future climates. J. Geophys. Res. 117, D22104. http://dx.doi.org/10.1029/2012JD018062.
Wood, A.W., Leung, L.R., Sridhar, V., Lettenmaie, D.P., 2004. Hydrologic implications of dynamical and statistical approaches to downscaling climate model outputs. Clim. Change 62, 189–216.
Xu, C.Y., 1999. From GCMs to river flow: a review of downscaling methods and hydrologic modelling approaches. Prog. Phys. Geogr. 23 (2), 229–249.
Xue, X., Hong, Y., Limaye, A.S., Gourley, J.J., Huffman, G.J., Khan, S.I., Dorji, C., Chen, S., 2013. Statistical and hydrological evaluation of TRMM-based multi-satellite precipitation analysis over the Wangchu Basin of Bhutan: are the latest satellite precipitation products 3B42V7 ready for use in ungauged basins? J. Hydrol. 499, 91–99.
Yatagai, A., Kamiguchi, K., Arakawa, O., Hamada, A., Yasutomi, N., Kitoh, A., 2012. APHRODITE: constructing a long-term daily gridded precipitation dataset for Asia based on a dense network of rain gauges. Bull. Am. Meteorol. Soc. http://dx.doi.org/10.1175/BAMS-D-11-00122.1.
Zhao, Q.D., Ye, B.S., Ding, Y.J., et al., 2013. Coupling a glacier melt model to the Variable Infiltration Capacity (VIC) model for hydrological modeling in north-western China. Environ. Earth Sci. 68 (1), 87–101. http://dx.doi.org/10.1007/s12665-012-1718-8.